Finite-time recurrence analysis of chaotic trajectories in Hamiltonian systems

Matheus S. Palmero, Iberê L. Caldas and Igor M. Sokolov

View Online   Export Citation   CrossMark

ARTICLES YOU MAY BE INTERESTED IN

AIP Publishing

Finite-time recurrence analysis of chaotic trajectories in Hamiltonian systems

Matheus S. Palmero,[1,2,a] Iberê L. Caldas,[1] and Igor M. Sokolov[2]

AFFILIATIONS

[1] Instituto de Física, Universidade de São Paulo, São Paulo, SP, Brazil
[2] Institut für Physik, Humboldt-Universität zu Berlin, Berlin, Germany

[a] **Author to whom correspondence should be addressed:** matheuspalmero@gmail.com

ABSTRACT

In this work, we show that a finite-time recurrence analysis of different chaotic trajectories in two-dimensional non-linear Hamiltonian systems provides useful prior knowledge of their dynamical behavior. By defining an ensemble of initial conditions, evolving them until a given maximum iteration time, and computing the recurrence rate of each orbit, it is possible to find particular trajectories that widely differ from the average behavior. We show that orbits with high recurrence rates are the ones that experience stickiness, being dynamically trapped in specific regions of the phase space. We analyze three different non-linear maps and present our numerical observations considering particular features in each of them. We propose the described approach as a method to visually illustrate and characterize regions in phase space with distinct dynamical behaviors.

Published under an exclusive license by AIP Publishing. https://doi.org/10.1063/5.0102424

Recurrence, as not only a fundamental characteristic of many dynamical systems, is also an intrinsic feature of stickiness phenomena. In non-linear Hamiltonian dynamics, stickiness happens when chaotic trajectories visit specific regions of phase space going through successive dynamical traps. We investigate the connection between different initial conditions, highly recurrent trajectories, and the stickiness phenomena considering three Hamiltonian maps. These are as follows: First, the well-studied standard map where the proposed recurrence analysis makes evident the inherent sensitivity on initial conditions of chaotic orbits. Second, the simplified Fermi-Ulam model where it is possible to find specific trajectories that differ from the average dynamical behavior of a large ensemble of initial conditions. And finally, the Ullmann map, a model for the magnetic field lines of a tokamak under suitable perturbation regimes, where we combine prior analyses to find relevant trajectories in phase space. Additionally, the outlined recurrence approach is proposed as a general method to study and characterize different regions of given phase spaces.

I. INTRODUCTION

Hamiltonian systems under small periodic perturbations have been studied for decades due to rich dynamical properties in both chaotic and regular motions.[1–6] In particular cases, these systems can be described by symplectic two-dimensional non-linear maps, which are often deliberately simplistic models for higher dimensional dynamical systems in many areas of science.[7–10]

The area-preserving phase spaces of such systems are composed by a local and/or global chaotic sea along with KAM islands of periodic dynamics.[11] These are called *mixed phase spaces*, where a chaotic orbit evolved from initial conditions (ICs) at the chaotic sea may experience different dynamical behaviors in a given maximum iteration time. In that sense, it is interesting to have a finite-time analysis on the evolution of a single orbit or an ensemble of orbits, in order to learn and describe exactly how is the chaotic evolution until a defined maximum iteration time.

Particularly for mixed phase spaces, there exist regions in which chaotic orbits spend a considerable amount of time experiencing successive dynamical traps. The trajectory, once free to explore all chaotic regions of phase space, is now temporally confined in a peculiar quasi-periodic motion in the vicinity around the stability islands. This is the well-known phenomenon of *stickiness*[12–17] that affects transport and statistical properties of chaotic orbits. In that sense, prior knowledge if a given trajectory will or will not experience stickiness is important. Although it is known that it depends on the (*i*) IC of the orbit and (*ii*) the control parameters of the system,

specifically why and when an orbit will experience stickiness are still open problems.[18] In this work, we explore (i), namely, the dependence on ICs.

In order to investigate the stickiness and other finite-time behaviors of Hamiltonian systems described via non-linear symplectic maps, we propose an approach based on the study of recurrence of a trajectory or an ensemble of trajectories of interest. It is common to define recurrence if at time t_j, a given trajectory $\boldsymbol{x}(t_j) \approx \boldsymbol{x}(t_i)$, with $(t_i < t_j)$, i.e., returns into the dynamical neighborhood of a previous state. Considering a threshold distance ε, it is possible to write a binary recurrence matrix (RM), composed by the elements $R_{i,j}$ defined as

$$R_{i,j}(\varepsilon) = \begin{cases} 1 \text{ if } \|\boldsymbol{x}(t_i) - \boldsymbol{x}(t_j)\| < \varepsilon \\ 0 \text{ otherwise,} \end{cases} \quad (1)$$

where $\| \cdot \|$ is a suitable norm. Every entry of 1 in the RM represents a recurrence of the analyzed trajectory, meaning that $\boldsymbol{x}(t_i)$ and $\boldsymbol{x}(t_j)$ are dynamically $\epsilon-$near to each other. Since we focus in a finite-time recurrence analysis, it is worth remarking that $0 < t_i < t_j \leq N$, where N is the trajectory's maximum iteration time. In that regard, RM is size $(N \times N)$.

The visual representation of the RM is known as the recurrence plot (RP). Usually, the RP depicts every null entry of the RM by a white pixel and the 1s entries by black pixels. The RPs can be very different, displaying particular recurrence patterns based on the evolved trajectory, which is determined by its IC. In addition, one RP may portray different dynamical behaviors for a given trajectory, considering its evolution up to N. For instance, a chaotic orbit initiated near periodic regions can produce similar recurrence patterns to a quasi-periodic motion. However, after a sufficient iterated time, this same trajectory can escape toward other chaotic regions of phase space, producing patterns-related pure chaotic motion. In this case, the RP would show us different recurrence patterns for distinct time windows until the dynamical evolution ends at the maximum iteration time.

Once the RP of a trajectory of interest is computed, there are many different measures that are able to quantify and differentiate several aspects between different RPs. These are called recurrence quantification analysis (RQA).[19,20] The simplest one is the recurrence rate (RR), which provides the percentage of recurrence points as follows:

$$RR = \frac{1}{N^2} \sum_{i,j=1}^{N} R_{ij}. \quad (2)$$

Note that $RR = RR(N)$, i.e., the recurrence rate depends on the maximum iteration time considered for the evolution of the given trajectory.

Due to the fundamental nature of the stickiness, as a trapped quasi-periodic motion eventually experienced by particular chaotic trajectories, the RR is a suitable measure[21,22] that can differentiate purely chaotic orbits from orbits that, indeed, experience stickiness in the considered time-frame. Moreover, stickiness has also been studied using tools from recurrence and extreme value theory.[23]

In this work, we study the finite-time chaotic dynamics via recurrence analysis in three different non-linear area-preserving maps: The standard map; the simplified Fermi-Ulam model, and the Ergodic limiter map or the Ullmann map. In each of them, we numerically investigate the presence of particular chaotic trajectories with high RR. We propose that it is possible to identify regions of high recurrence in phase space and connect them to the phenomena of stickiness. Additionally, we show that it is possible to compute RR of an ensemble of trajectories and infer that there are specific ICs that lead to trajectories that will certainly experience stickiness considering their finite-time evolution.
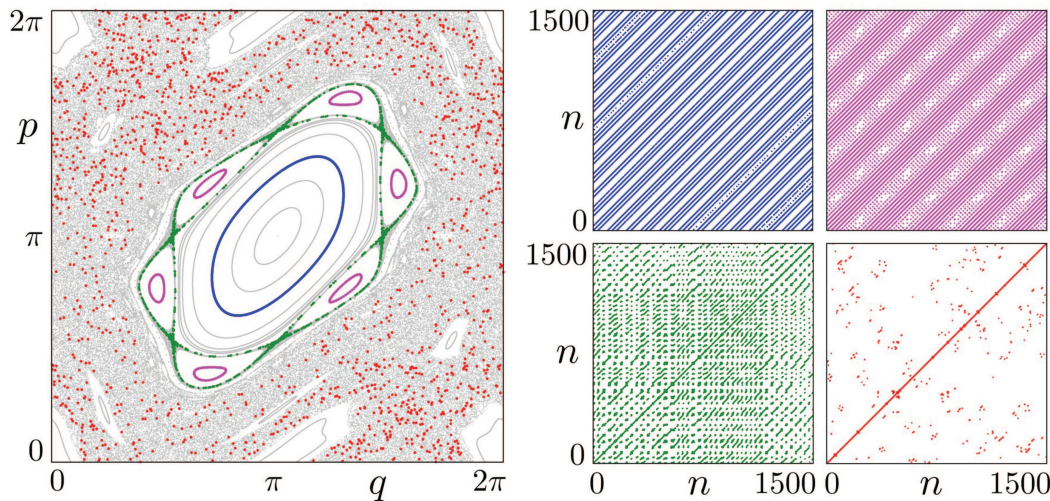

FIG. 1. Phase space of the SM with $k = 1.46$, along with four different trajectories in colors (left). RPs with threshold distance $\varepsilon = 0.05$ of the selected four trajectories evolved until $N = 1500$ iterations (right).

The work is structured as follows: In Sec. II, we review the three models, showing their characteristic phase spaces along with four different orbits and their respective RPs. In Sec. III, we present numerical observations provided by the finite-time recurrence analysis in each one of the models. Finally, we make a general discussion and draw our conclusions in Sec. IV.

II. PHASE SPACES AND RECURRENCE PLOTS

This section is devoted to reviewing and presenting some general aspects of the three selected models. In the first sub-section, we review the standard map, one of the most studied area-preserving non-linear maps. In the second, the simplified Fermi-Ulam model, a toy model of astrophysics background. And finally, the third sub-section is devoted to the Ergodic limiter map or the Ullmann map, a non-linear symplectic map that models the magnetic field lines of a tokamak equipped with an ergodic limiter.

A. Standard map

The standard map (SM), also known as the Chirikov–Taylor map,[24] can be used to describe the motion of a particle constrained to a movement on a ring while kicked periodically by an external field. It is possible to define a symplectic non-linear discrete map T_{SM} to investigate the dynamics via extensive numerical simulations.

The mapping $T_{SM}(p_n, q_n) = (p_{n+1}, q_{n+1})$ gives the position and momentum for the $(n+1)th$ iteration by the following equations:

$$T_{SM} : \begin{cases} p_{n+1} = p_n + k\sin(q_n) \quad \mod (2\pi) \\ q_{n+1} = q_n + p_{n+1} + \pi \quad \mod (2\pi), \end{cases} \quad (3)$$

where the parameter k controls the intensity of the non-linearity and the added term $+\pi$, on the equation for q_{n+1}, is to centralize the main island on phase spaces. It is also important to mind that this is

an area-preserving map since the determinant of its Jacobian matrix is equal to unity.

In all of our numerical simulations of the SM, we fixed the parameter $k = 1.46$. The resulting mixed phase space is depicted in the left panel of Fig. 1. Additionally, we selected four different orbits, evolved up to $N = 1500$, in distinct regions of phase space and computed their respective RP, portrayed in the right panels of Fig. 1.

The RPs depicted in the right panels of Fig. 1 show different patterns associated with the distinct types of dynamics present in the mixed phase space of the SM. First, in blue, we see the diagonal lines of pure periodic motion of an orbit placed on an invariant curve inside of the central island. Then, in magenta, we see more separated diagonal lines, also indicating pure periodic dynamics, but for an orbit placed inside a secondary, period 6, chain of islands. In green, however, we see peculiar recurrence patterns of complex dynamics associated with the well-confined chaotic layer between the islands' chain. Finally, in red, we see the behavior of a chaotic orbit placed far enough in the chaotic sea that surrounds all phase space.

B. Simplified Fermi-Ulam model

The simplified Fermi-Ulam model (SFUM) is a version of the Fermi accelerator, which was originally introduced by Enrico Fermi as a possible explanation for the production of very high-energy cosmic rays.[25] Its acceleration mechanism involves the repulsion of an electrically charged particle by strong oscillatory magnetic fields, a process that is analogous to a classical particle colliding elastically with an oscillating physical boundary.[5,26,27] It is a conservative model that consists basically of a particle bouncing back and forth between two rigid walls, one of which is fixed, whereas the other moves periodically in time with a normalized amplitude κ.
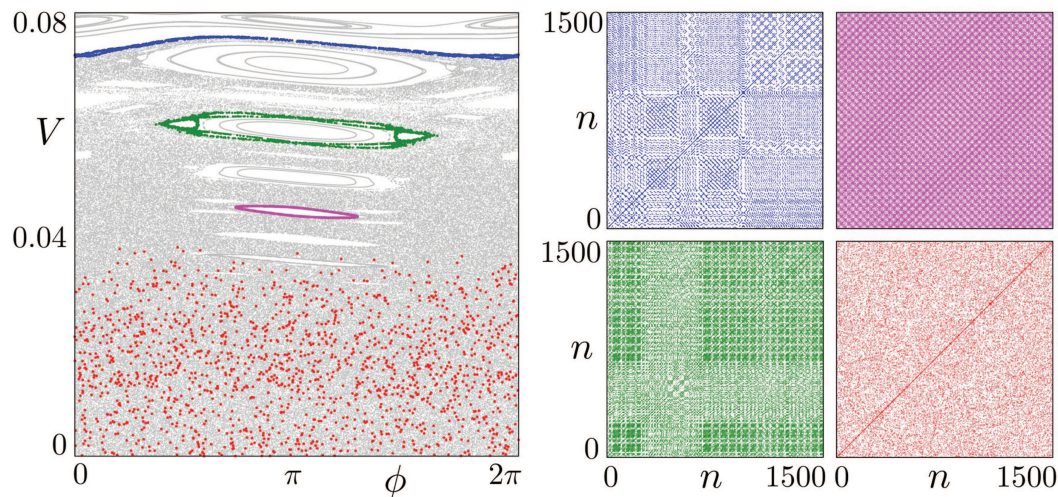

FIG. 2. Phase space of the SFUM with $\kappa = 0.001$, along with four different trajectories in colors (left). RPs with $\varepsilon = 0.05$ of these four trajectories evolved until $N = 1500$ iterations (right).

The dynamical system is described by a two-dimensional, nonlinear, area-preserving map $T_{SFUM}(V_n, \phi_n) = (V_{n+1}, \phi_{n+1})$. The velocity of the particle is the action variable and the phase, related to the time-dependent boundary, is the angle variable. Taking into account that the absolute value of velocity changes at the moment of each collision, the mapping for the simplified version can be obtained if we approximate the oscillating wall as fixed, but when the particle suffers a collision, it changes its momentum as if the wall were moving. This simplified version is valid when the non-linear parameter κ is relatively small ($\kappa < 0.01$). Hence, the map of the SFUM is

$$T_{SFUM} : \begin{cases} V_{n+1} = |V_n - 2\kappa \sin(\phi_n)| \\ \phi_{n+1} = \phi_n + 2/V_{n+1} \mod (2\pi). \end{cases} \quad (4)$$

The term $2/V_{n+1}$ corresponds to the time between collisions and $-2\kappa \sin(\phi_n)$ gives the gain or loss of velocity in each collision.

The phase space $V \times \phi$ for the FUM is mixed type, composed of a chaotic sea and KAM islands. In addition, it is bounded by an invariant spanning curve that plays the role of a boundary: trajectories of lower velocity will never visit a region above this curve, no matter how many times the trajectory is iterated. A characteristic phase space of the SFUM, considering $\kappa = 0.001$, is shown in the left panel of Fig. 2.

Similarly to the SM, the four right panels in Fig. 2 depict regions of distinct dynamics present in phase space of the SFUM. In blue, we see the complex behavior of a chaotic orbit placed in close vicinity of the invariant spanning curve that bounds the chaotic sea. In magenta, we see pure periodic behavior of an orbit inside one of the central KAM islands. In green, we see a complex dynamics of a chaotic orbit placed close enough to another center KAM island.

Finally, in red, we see the behavior of a chaotic orbit placed far on the chaotic sea.

C. Ergodic magnetic limiter map

The ergodic magnetic limiter map or Ullmann map (UM) was proposed as a symplectic two-dimensional non-linear map that models the magnetic field lines of a tokamak assembled with an ergodic limiter.[28] Tokamaks are toroidal shape machines that magnetically confine plasma in order to produce controlled thermonuclear fusion power.[29] Inside the torus, in the plasma core, the magnetic field is strong and stable enough for the duration of a typical tokamak discharge. However, on the plasma edge, closer to the inner walls of the machine, the magnetic field lines are often perturbed, forming regions of strong instabilities. In many cases, to either control or change the magnetic configuration in this outer region, the tokamak is assembled with devices placed at the border of the machine. This is the case of ergodic magnetic limiters that are, basically, outer rings of coils with helical electric current that periodically perturbs the magnetic field lines at the plasma edge.

The UM is a fitting symplectic model because it can be derived from a suitable generating function, the profile of the safety factor $q(r)$ is freely adjustable for a given discharge, and the parameters of the model are directly linked to experimental parameters of a tokamak, such as the intensity of the toroidal magnetic field B_0, large radius R_0, small radius b, and radius of the plasma column a. For complete derivation and additional details regarding the UM, see Refs. 28 and 30.

The full model is a composition of two maps $T_{UM}^{eq} \circ T_{UM}^{pert}(y_n, x_n) = (y_{n+1}, x_{n+1})$, where our variables (y, x) are the dimensionless radius and poloidal angle, respectively, given by $y = 1$
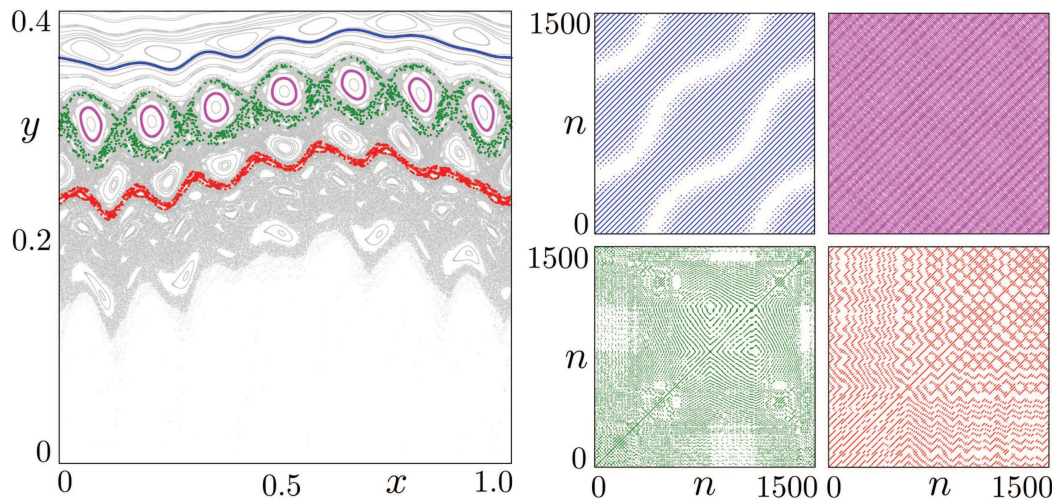

FIG. 3. Phase space of the UM with $\delta B = 1.50\%$, along with four different trajectories in colors (left). RPs with $\varepsilon = 0.05$ of the selected four trajectories evolved until $N = 1500$ iterations (right).

$- r/b$, and $x = \theta/2\pi$. The first part $T_{\text{UM}}^{\text{eq}}$ is the equilibrium dynamics with a toroidal correction, given by the following equations:

$$T_{\text{UM}}^{\text{eq}} : \begin{cases} y_{n+1}^* = \dfrac{y_n}{1 - a_1 \sin(x_n)} \\ x_{n+1}^* = x_n + \dfrac{2\pi}{q^0(y_{n+1}^*)} + a_1 \cos(x_n), \end{cases} \quad (5)$$

where $a_1 = -0.04$ is the first term of the toroidal correction proposed by Ullmann and $q^0(y)$ is the equilibrium safety factor calculated via the Ampère law from a given radial profile of the poloidal magnetic field.[28] The second part $T_{\text{UM}}^{\text{pert}}$ is considering the periodic perturbation caused by the ergodic magnetic limiter given by the following equations:

$$T_{\text{UM}}^{\text{pert}} : \begin{cases} y_n = y_{n+1}^* + \dfrac{m}{m-1} C(1 - y_n)^{m-1} \sin(mx_n^*) \\ x_{n+1} = x_n^* - C(1 - y_n)^{m-2} \cos(mx_n^*), \end{cases} \quad (6)$$

where m is the number of coils in the magnetic limiter and C is a dimensionless constant that shows the relation between the parameters as follows:

$$C = \frac{2\pi}{q_a} \left(\frac{b}{a}\right)^{m-2} \delta B, \quad (7)$$

where $q_a = q^0(y = 1 - a/b)$ is the value of the safety factor at the plasma column ($r = a$) and δB is our actual control parameter in numerical simulations. It denotes intensity of the relative poloidal perturbation in the magnetic field, which is defined as

$$\delta B = \frac{B_{ex}}{B_\theta(a)}, \quad (8)$$

where B_{ex} is the intensity of the external magnetic field caused by the ergodic limiter and $B_\theta(a)$ is the intensity of the poloidal magnetic field calculated at the border of the plasma column ($r = a$).

With that, all the parameters can be set for a specific tokamak. Here, we use the parameters of the TCABR, the tokamak of the Physics Institute, University of São Paulo,[31] and it is possible to model the configuration of the magnetic field via phase space of the UM. The values of the parameters are as follows: $B_0 = 1.2$ T, $R_0 = 0.61$ m, $b = 0.18$ m, $a = 0.22$ m, $m = 7$, and $q_a = 5$. The typical phase space of the UM is shown in Fig. 3, considering a relative perturbation strength of $\delta B = 1.50\%$. On Fig. 3, we depict only the outer region $y < 0.5$ of phase space, where the perturbation of the magnetic field is visible.

Analogously to the SM and SFUM, the four right panels in Fig. 3 depict distinct dynamical behaviors present in phase space of the UM. In blue, we see an orbit placed on an invariant spanning curve, where a different periodic motion is depicted by long diagonal lines wrapped in an oscillatory pattern. In magenta, we see pure periodic dynamics of an orbit inside a period 7 KAM islands. In green, we see complex dynamics of a chaotic orbit placed on the chaotic region around the period 7 chain of islands. Furthermore, in red, we see unique quasi-periodic behavior of a chaotic orbit placed in a vicinity of a region with many small islands.

III. NUMERICAL OBSERVATIONS

In this section, we explore some numerical results showing particular aspects of the three selected models. First, for the SM, we found a distinguishing region of the chaotic sea that illustrates a strong sensitivity to ICs of two chaotic orbits. This region is further investigated for an ensemble of trajectories and its recurrence quantification, namely the *RR*. In the second subsection, we analyze
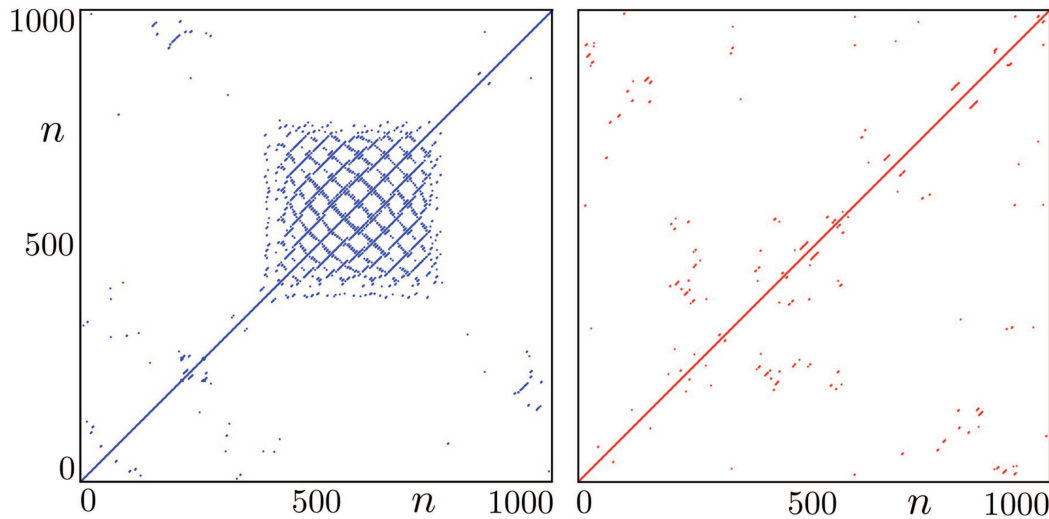
FIG. 4. RPs with $\varepsilon = 0.05$ for two chaotic trajectories of the SM with very close ICs. In blue, the trajectory started at $(q_0^*, p_0^*) = (0.512\,345\,678\,998\,70, \pi)$ (left), and in red, the trajectory started at $(q_0^* + 1 \times 10^{-14}, p_0^*)$ (right).
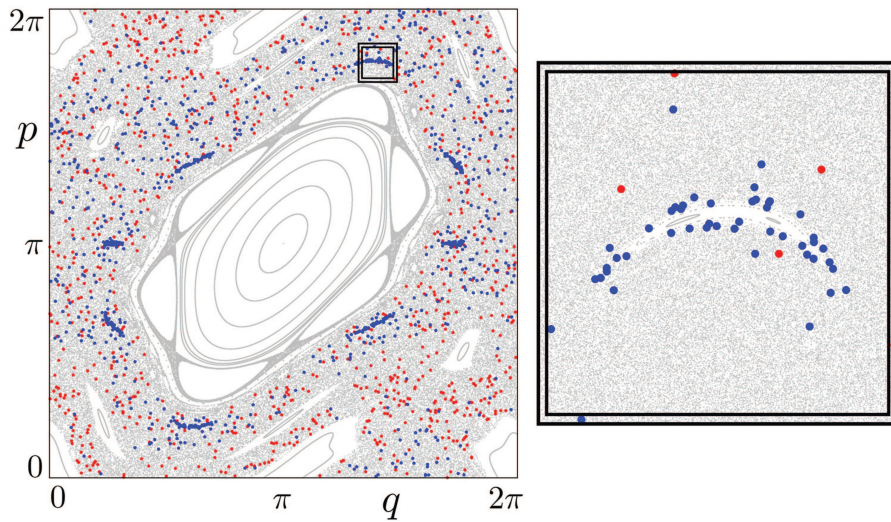
FIG. 5. Phase space of the SM for $k = 1.46$ along with the selected chaotic trajectories depicted in red and blue. The black square displays the amplified region around a small island in the chaotic sea.

the behavior of a broad ensemble of ICs on the chaotic region of the SFUM. We characterize the different behaviors between all trajectories from the ensemble also via their *RR*, differentiating the ones with high and low *RR*. Finally, in the last subsection, we explore the behavior of an ensemble of trajectories placed in close vicinity of an unstable periodic orbit (UPO) of the UM. We display the RPs of particular trajectories selected by its *RR*, revealing unique patterns of periodic, quasi-periodic, and chaotic behaviors in the considered time-frame.

A. Standard map—Strong sensitivity to ICs

In order to study the influence of ICs on the dynamics of chaotic orbits, we selected two extremely close ICs and evolve them until $N = 1000$ iterations of the SM. The selected IC for the first trajectory is $(q_0, p_0) = (q_0^*, p_0^*) = (0.512\,345\,678\,998\,70, \pi)$ and for the second is $(q_0, p_0) = (q_0^* + 1 \times 10^{-14}, p_0^*)$. So, $p_0 = \pi$ is fixed for both trajectories, but q_0 changes only by 10^{-14}. It is important to have high precision on (q_0, p_0) to be able to investigate the dynamics while considering only small differences in
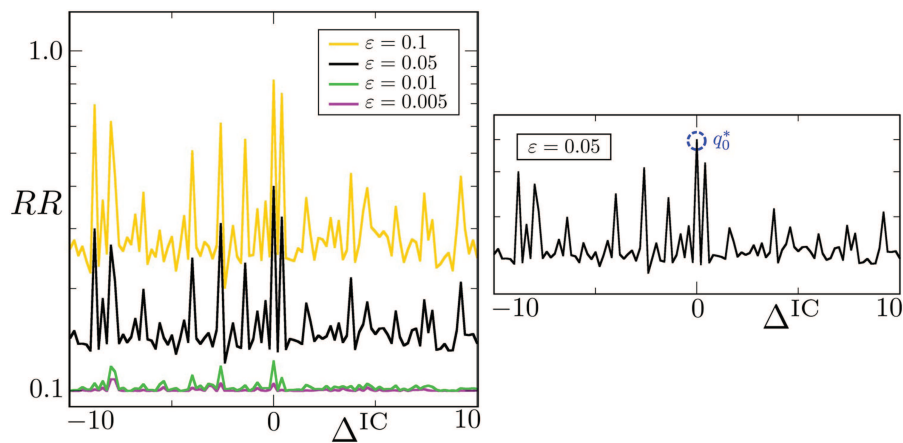
FIG. 6. *RR* in log scale, as a function of the defined relative distance Δ^{IC} for the ensemble around (q_0^*, p_0^*) in the SM. The different colors are for different values of the threshold recurrence distance ε. The right panel is specifically for $\varepsilon = 0.05$, where the peak at $\Delta^{IC} = 0$ is highlighted by the blue dashed circle.
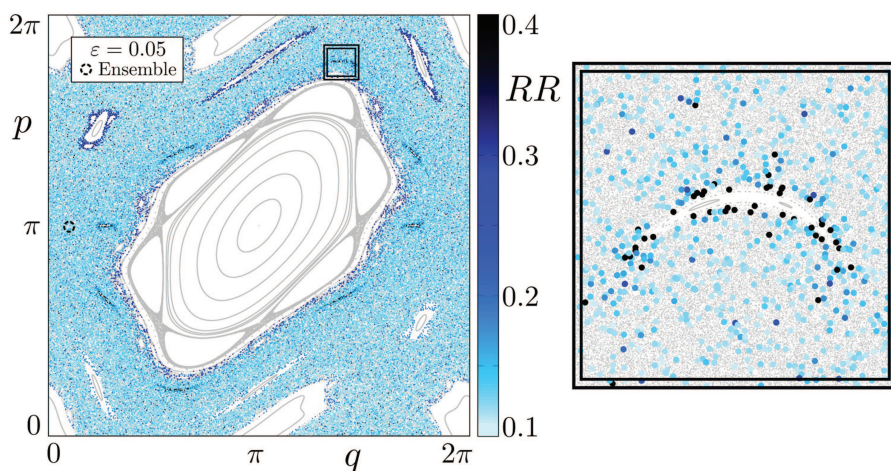
FIG. 7. Phase space of the SM along with 100 trajectories from the ensemble E. The ICs of E are placed in the highlighted dashed circle (out of scale). The color axis shows the computed RR for each one of the trajectories, considering $\varepsilon = 0.05$ and $N = 1000$. The black square displays the amplified region around a small island in the chaotic sea.

their ICs. First, we show on Fig. 4 the RPs for these two trajectories.

It is clear from Fig. 4 that the RPs are different, in spite of the proximity of these two ICs. The first one, depicted in blue, exhibits an interesting recurrence pattern around 500 iterations, differing from the red trajectory where this pattern is absent. Additionally, the blue trajectory changes its dynamical behavior from initially chaotic, to quasi-periodic, then to chaotic again in an intermittent manner.

In Fig. 5, we show the characteristic phase space of the SM along with these two selected trajectories, both depicted by its colors predefined in Fig. 4. It is possible to visualize that indeed these two chaotic trajectories visit different regions of phase space. The orbit depicted in red does not concentrate in any region of the space, as a visual evidence of its pure chaotic dynamics. However, the blue orbit concentrates in a particular region around a small chain of islands in the chaotic sea, as observed by the amplified region on
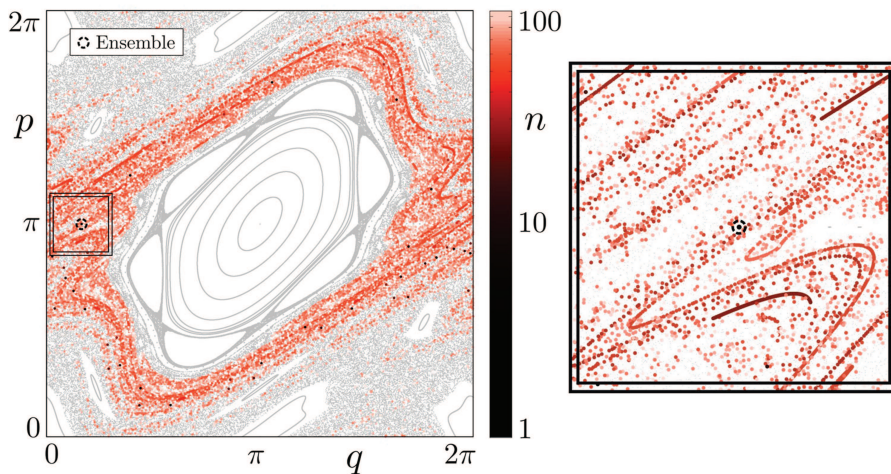

FIG. 8. Evolution of an ensemble of 1000 ICs in the phase space of the SM. The ensemble's initial position is highlighted by the dashed circle (out of scale). The color axis shows the iteration time in log scale for all trajectories. The region around the ICs is amplified on the highlighted square.
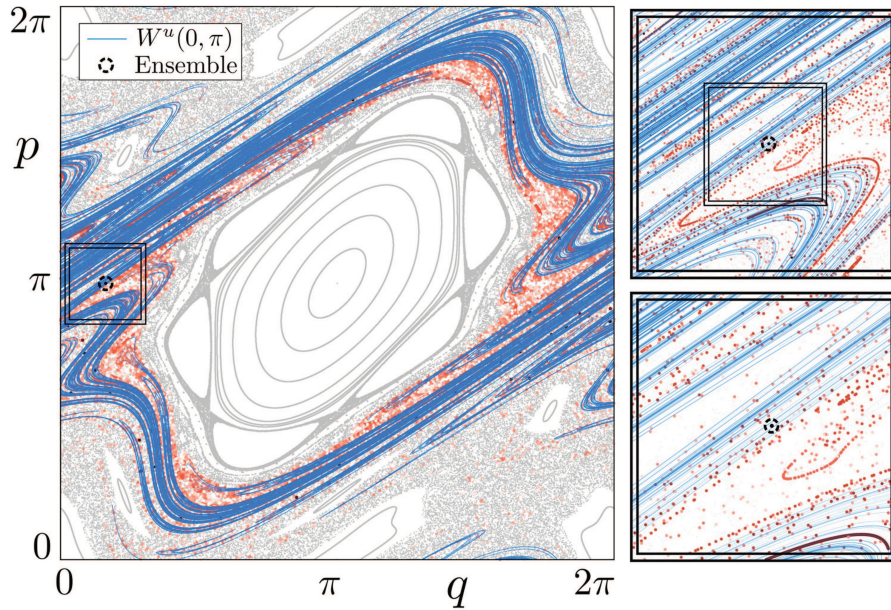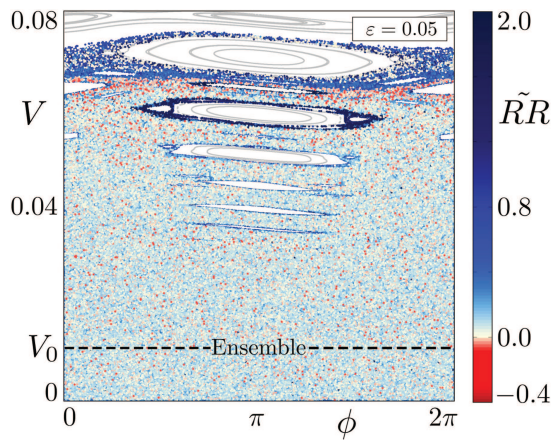
FIG. 9. Phase space of the SM along with the ensemble's trajectories in red and the invariant unstable manifold $W^u(0, \pi)$ in blue. The ensemble's initial position is highlighted by the dashed circle (out of scale). The highlighted black squares show subsequent amplifications of the region around the ensemble of ICs.

the black highlighted square. This is clear evidence of the stickiness phenomena, as the blue orbit gets dynamically trapped nearby a KAM island for approximately 250 iterations. Furthermore, as also observed in Fig. 4, the blue orbit is more recurrent than the red orbit, as it returns almost periodically to the vicinity of the island in this trapped time.

Continuing the investigation on the dependence of ICs, we now place an ensemble E of 100 ICs in the very close vicinity of (q_0^*, p_0^*). The $p_0^E = \pi$ is again fixed for the whole ensemble, but $q_0^E \in [q_0^* - 10^{-14}, q_0^* + 10^{-14}]$, i.e., the ensemble is formed by a very small line around (q_0^*, p_0^*). We define $\Delta^{IC} = (q_0^E - q_0^*) \times 10^{13}$ as a relative distance between the ensemble's initial conditions.[32]
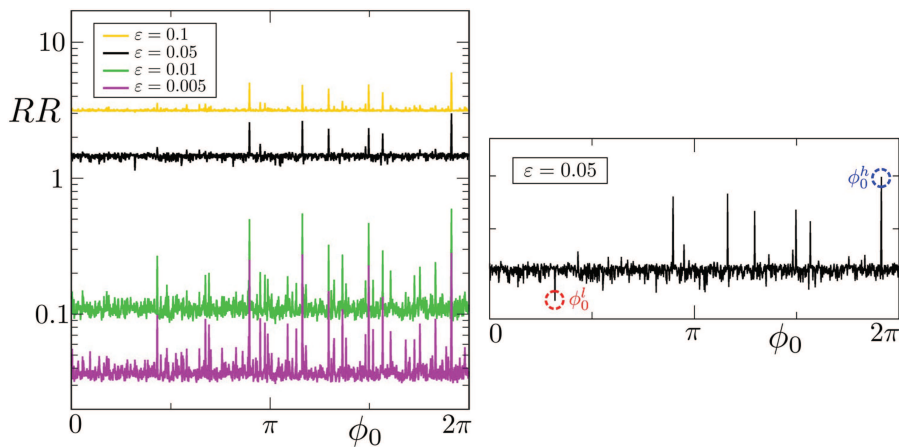
FIG. 10. RR in log scale, as a function of the initial phase ϕ_0 for 1000 ICs in the ensemble at $V_0 = 0.01$ in the SFUM. The different colors are for different values of the threshold distance ε. The right panel is specifically for $\varepsilon = 0.05$, where the highest and lowest values are highlighted by the blue and red dashed circles, respectively.

FIG. 11. Phase space of the SFUM for $\kappa = 0.001$ along with the 1000 trajectories from the ensemble E. The color axis shows $\tilde{RR}$ for each one of the trajectories, considering $\varepsilon = 0.05$ and $N = 10^4$. Regions in light-yellow have average value of recurrences, regions in red have low recurrence, and regions in dark-blue have high recurrence.

As previously mentioned, the RR is a suitable recurrence quantification while analyzing chaotic trajectories that may experience stickiness. In that sense, we computed the RR for all trajectories of E defined above. The values of the computed RR in function of the relative distance Δ^{IC} are shown in Fig. 6.

Analyzing RR for all trajectories of E as a function of its ICs helps us identify the ICs' exact coordinates of highly recurrent orbits. The high and low values of RR in Fig. 6 also suggest a scaling

behavior as they agree for different values of the threshold recurrence distance ε. This scaling behavior will be addressed more suitably in another opportunity. In particular, the peaks at $\Delta^{IC} = 0$, present in all analyzed scales, refer to $q_0 = q_0^*$, the one of the blue RPs in Fig. 4. In addition to this analysis, it is possible to show phase space of the SM along with all trajectories from E and in the color scale the computed RR for each trajectory. Figure 7 displays the result.

The analysis of the computed RR for all the trajectories in E on phase space of the SM supports the idea that trajectories with high RR are indeed the ones that experience stickiness in the given maximum iteration time $N = 1000$. As observed in Fig. 7, regions near the KAM islands are surrounded by highly recurrent orbits, depicted by dark-blue colors. Particularly, the same highlighted region as in Fig. 5 shows the highest value of RR, meaning that indeed the trajectory's IC with higher RR is exactly (q_0^*, p_0^*), as also can be verified in Fig. 6.

Finally, as a possible explanation of why this region around (q_0^*, p_0^*) is so sensitive, we increase the number of ICs on the ensemble to 1000 and evolve it until only 100 iterations of the SM. The ensemble's initial position is the same as before, $p_0^E = \pi$ and $q_0^E \in [q_0^* - 10^{13}, q_0^* + 10^{13}]$. Figure 8 shows how this larger ensemble evolves, as the beginning of the dynamics is depicted by dark-red and the last iterations are depicted in light-red colors.

It is possible to notice that the ensemble evolves following certain preferable regions of phase space, as the dark-red colors, visible at the amplified square, forms specific straight and curved lines. This indicates that there are hidden structures in phase space that influence the dynamics. These structures are invariant manifolds associated with UPOs in the system.

In general terms, let T be a two-dimensional invertible map, with both T and T^{-1} differentiable, and let $\boldsymbol{o}$ be an UPO of the mapping T. The unstable invariant manifold W^u associated with $\boldsymbol{o}$
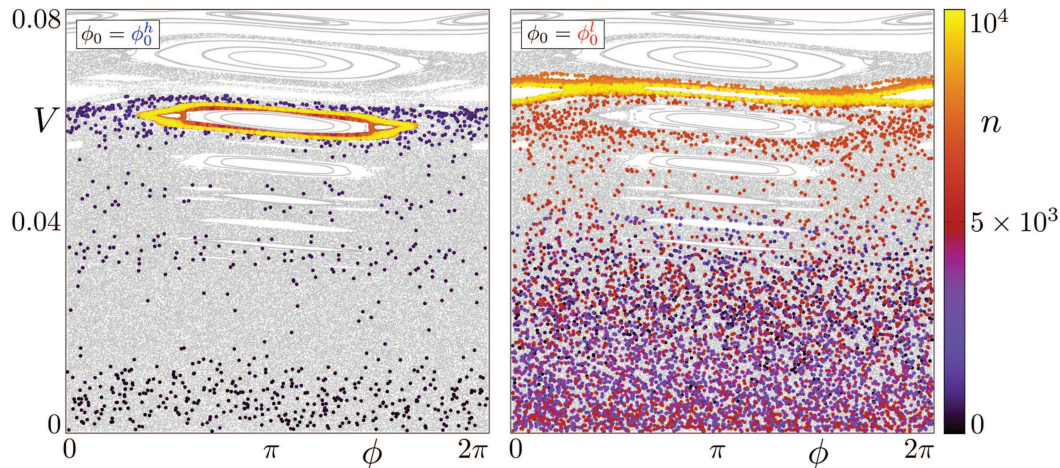
FIG. 12. Evolution of the orbits started at $\phi_0 = \phi_0^h = 6.006\,448\,416\,773\,389\,8$ (left) and $\phi_0 = \phi_0^l = 1.000\,026\,490\,331\,884\,1$ (right) on the phase space of the SFUM, considering $V_0 = 0.01$ for both. The color axis shows the iteration time of the trajectories.
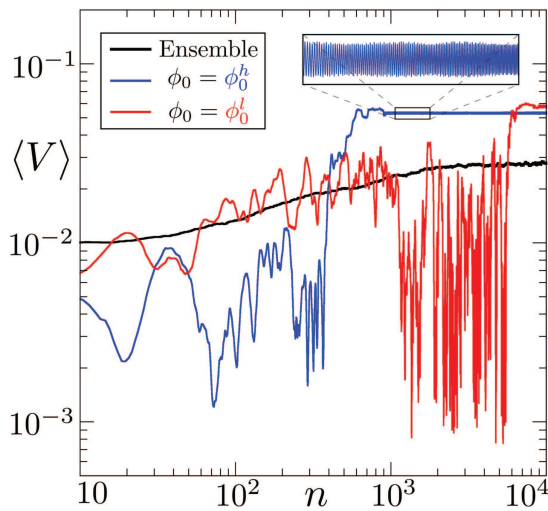
FIG. 13. Behavior of the average velocities in the function of iterations in a log-log scale for the SFUM. In black is depicted the average behavior over all the ensemble, in blue is the moving average of the orbit with $\phi_0 = \phi_0^h$, and in red the moving average of the orbit with $\phi_0 = \phi_0^l$. The inset shows an amplified region of the quasi-periodic behavior of the blue orbit.

is defined as

$$W^u(\boldsymbol{o}) = \{\boldsymbol{x} \in U \subset \mathbb{R}^2 \mid T^{-n}(\boldsymbol{x}) \to \boldsymbol{o} \text{ as } n \to \infty\}, \quad (9)$$

where $\boldsymbol{x}$ is the pair of the defined coordinates and U is a subset $\mathbb{R}^2$ that in practice can be a region of system's phase space.[33,34] Knowing
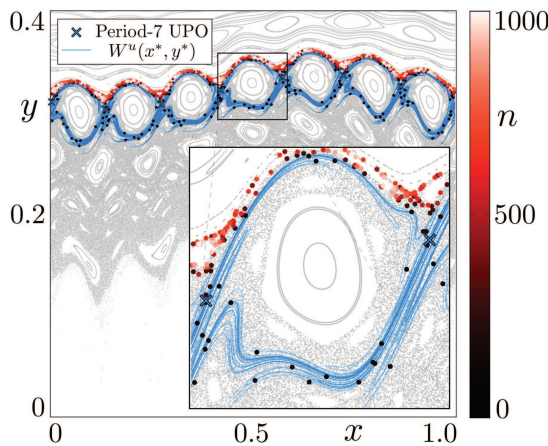
FIG. 14. Outer region of the phase space of the UM for $\delta B = 1.50\%$, with the period 7 UPO in blue-black x-points, the associated unstable invariant manifold in blue, and the evolution of a single orbit placed at $(x_0, y_0) = (1.724\,770\,290\,893\,000\,0, y^*)$ in color. The color scale depicts the orbit's iterations. The inset shows the region around the KAM island amplified.

that the SM has an UPO at $(0, \pi)$, we use the method outlined in Ref. 35 to be able to trace the invariant unstable manifold of this UPO $W^u(0, \pi)$. Then, in Fig. 9, we show phase space with ensemble's evolution, as shown in Fig. 8, along with the numerically calculated invariant unstable manifold for visual comparison.

As expected, based on the initial dynamical behavior of this larger ensemble, the region around (q_0^*, p_0^*) is highly influenced by the outlined invariant manifold. Particularly, this is a region where we find long erratic unstable branches of the invariant manifold, which are, by definition, part of a fractal set that can be observed on successive amplifications in Fig. 9. This suggests that ICs with an infinitesimal difference, placed in this region of the chaotic sea, may follow completely different branches of the manifold, passing through different regions of phase space, thus experiencing distinct dynamics. This is evidence of the well-known sensitivity on ICs of chaotic trajectories, a hallmark of chaos theory.

B. Simplified Fermi-Ulam model—Phase ensemble

In order to further investigate the relation between different ICs, stickiness, and highly recurrent trajectories, we now consider the SFUM. This is a suitable system to study chaotic orbits because its phase space is well divided into a region of a broad chaotic sea for low velocities and a mixed region with chaos and KAM islands for higher velocities. In that sense, we begin our analysis considering the same approach presented in Fig. 6. Considering an ensemble E of 1000 ICs, placed at $V_0^E = V_0 = 0.01$, and $\phi_0^E \in [0, 2\pi]$, i.e., a line at the chaotic sea, at height $V = 0.01$ in phase space with uniformly distributed ICs all over the phase ϕ axis. We evolve these 1000 chaotic trajectories up to $N = 10^4$ iterations of the SFUM, calculating their respective RR. Figure 10 shows the result.

Analogously to the analysis for the SM, the scaling behavior could be also present here while considering the selected values of ε. Additionally, for $\varepsilon = 0.05$ displayed at the right panel in Fig. 10, there are particular values of the initial phase ϕ_0 that have high (ϕ_0^h) and low (ϕ_0^l) values of recurrence. These particular ICs will be analyzed further on. Initially, let us define a corrected recurrence rate as $\widetilde{RR} = RR - \langle RR \rangle$, where $\langle RR \rangle$ is the average over the ensemble. For $\varepsilon = 0.05$, $\langle RR \rangle = 1.459\,71$. $\widetilde{RR}$ is easier to identify trajectories that differ from the average behavior, allowing us to make the same analysis as in Fig. 10 but now with different colors for high and low RR. Figure 11 shows phase space of the SFUM with all trajectories from E colored by their respective corrected RR.

Again, the result shown in Fig. 11 corroborates the idea that trajectories with high RR are the ones that experience stickiness in the given maximum iteration time $N = 10^4$ for the SFUM. In addition, now it is possible to observe the areas explored by the orbits with low recurrences that are essentially well distributed over the chaotic sea. Furthermore, considering again the fixed value for $V_0 = 0.01$ for both, with $\phi_0 = \phi_0^h$ and $\phi_0 = \phi_0^l$, it is possible to visualize the evolution of those two particular trajectories on phase space. This is shown in Fig. 12.

From Fig. 12, it is clear that these two trajectories have completely different dynamical behaviors. In one hand, considering $\phi_0 = \phi_0^h$, the orbit rapidly goes toward one of the central KAM islands, where it gets trapped for a long time, as seen in the left panel of Fig. 12. In another hand, for $\phi_0 = \phi_0^l$, the orbit explores the
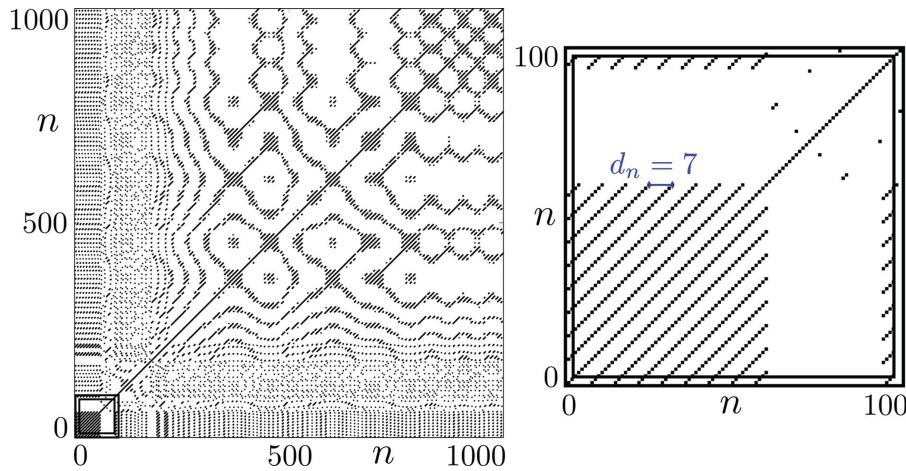
FIG. 15. RP of the orbit started at $(x_0, y_0) = (1.724\,770\,290\,893, y^*)$ with $\varepsilon = 0.05$ and up to $N = 1000$ iteration of the UM. The highlighted back square amplifies the RP for the first 100 iterations. In blue is the distance between the initial diagonal lines.

chaotic sea noticeably more than the orbit for ϕ_0^h, and it goes toward a different region by the end of its iterations. Comparing Fig. 12 with Fig. 11, there is not only a correlation between regions of high $\tilde{RR}$ and the orbit with $\phi_0 = \phi_0^h$, but also regions of low $\tilde{RR}$ and the orbit with $\phi_0 = \phi_0^l$.

As a final analysis regarding the differences between the orbits started at ϕ_0^h and ϕ_0^l in the SFUM, we can verify the dynamical behavior of the average velocity over the ensemble E, comparing it to a moving average of velocities for those two orbits. Figure 13 shows this comparison.

The average velocity over E, depicted by the black line in Fig. 13, presents an initial constant plateau at $V_0 = 0.01$ until

around 70 iterations, then it increases up to 10^3 iterations and it saturates in a higher plateau at $V \approx 0.03$. This dynamical behavior for the average velocity agrees with other findings for the SFUM.[26,36] Additionally, comparing the orbits depicted by red and blue lines, the difference is evident while considering the last decade of the log–log scale, namely, from 10^3 to 10^4. While the red orbit exhibits rather chaotic behavior, the blue one is trapped around one of the central KAM islands, exhibiting a strong quasi-periodic behavior until the end of its evolution. It is also worth mentioning that the red orbit ends in a higher plateau compared to the blue one, which can also be observed in Fig. 12.
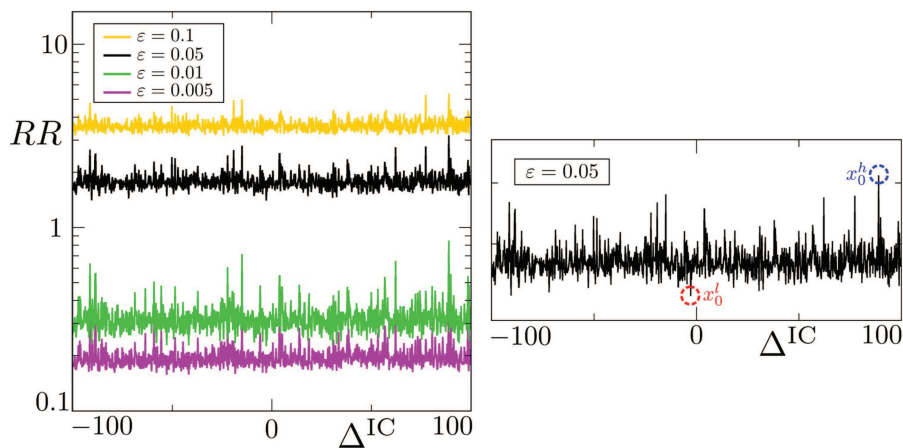
FIG. 16. RR in log scale, as a function of the relative distance Δ^{IC} for 1000 ICs in the ensemble at $y_0 = y^*$ in the UM. The different colors are for different values of the threshold distance ε. The right panel is specifically for $\varepsilon = 0.05$, where the highest and lowest values are highlighted by the blue and red dashed circles, respectively.
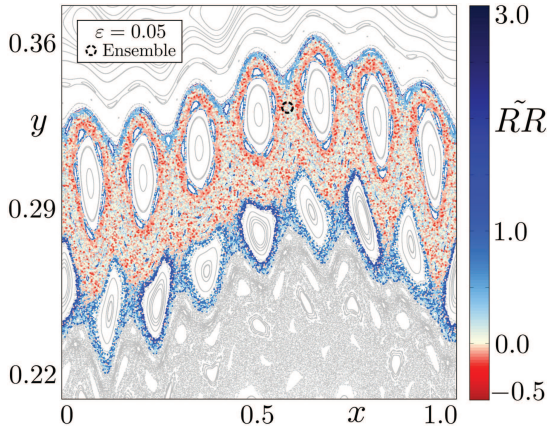
FIG. 17. Amplified phase space of the UM along with 1000 trajectories from the ensemble E. The ICs of E are placed in the highlighted dashed circle (out of scale). On the color axis is the computed $\tilde{R}R$ for each one of the trajectories, considering $\varepsilon = 0.05$ and $N = 1000$. Regions in light-yellow have average value of recurrences, regions in red have low recurrences, and regions in dark-blue have high recurrence.

C. Ergodic magnetic limiter map—UPO neighborhood

As a final example of this finite-time study on chaotic orbits in Hamiltonian systems via its recurrences' quantification, we analyze a special region of the UM. This is the first outer region of strong mixed behavior after the areas of stable magnetic field lines, where a period 7 chain of islands can be found, surrounded

by a relatively large chaotic sea. It is known that a stable periodic orbit, found in the center of a KAM island, has its counterpart as an unstable periodic orbit that can be found in the chaotic sea.[4] In that sense, we employ again the method outlined in Ref. 35 and numerically found the period 7 UPO with high computational precision. The position of this UPO is (x^*, y^*) = (1.724 770 290 893 414 8, 0.308 014 941 802 154 5).

Once the exact position of the UPO is calculated, it is possible to compute the invariant unstable manifold $W^u(x^*, y^*)$ associated with it. Additionally, we select as an IC (x_0, y_0) = (1.724 770 290 893 000 0, 0.308 014 941 802 154 5) to evolve as an orbit of interest. This particular orbit starts at the position of the UPO up to the 10^{-12} precision on the x variable and up to 10^{-16} precision on y variable. The discrepancy between x and y precision is due to the upcoming ensemble analysis in this neighborhood, where $y_0 = y^*$ will be fixed while changing x_0. Figure 14 shows phase space of the UM with the computed period 7 UPO, unstable manifold, and the evolution of the particular orbit.

Since now we are dealing with a higher period UPO, the definition of the invariant unstable manifold presented in Eq. (9) needs to be slightly amended. Let again T be a two-dimensional invertible map, with both T and T^{-1} differentiable, and let $\xi = \{o_1, o_2, \ldots, o_m\}$ be an UPO of period m of mapping T. The invariant unstable manifold W^u associated with ξ is given by

$$W^u(\xi) = \{x \in U \subset \mathbb{R}^2 \mid T^{-n}(x) \to T^{-n}(o_i) \text{ as } n$$
$$\to \infty, \, i = 1, \ldots, m\}, \qquad (10)$$

where again x is the pair of coordinates and U can be in practice a region of the system's phase space.

It is possible to note that the evolved orbit displayed in Fig. 14 closely follows the outlined path of W^u until at least 100 iterations, depicted by black points. Then, the orbit escapes from this specific path and explores an upper region of the chaotic sea, as evidenced
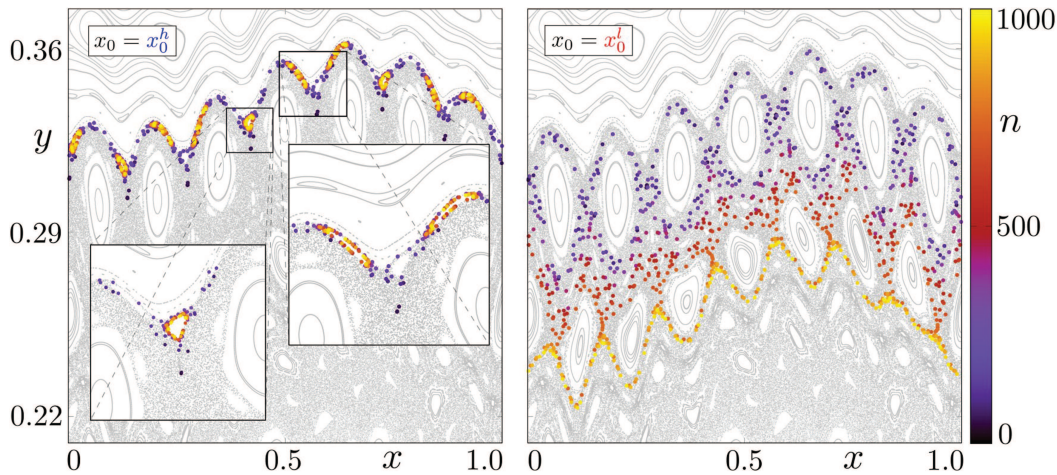
FIG. 18. Evolution of the orbits with $x_0 = x_0^h = 1.724\ 770\ 290\ 893\ 888$ (left) and $x_0 = x_0^l = 1.724\ 770\ 290\ 892\ 971$ (right) on the phase space of the UM, considering $y_0 = y^*$ for both. The color axis shows the iteration time of the trajectories and the insets amplified regions of interest.
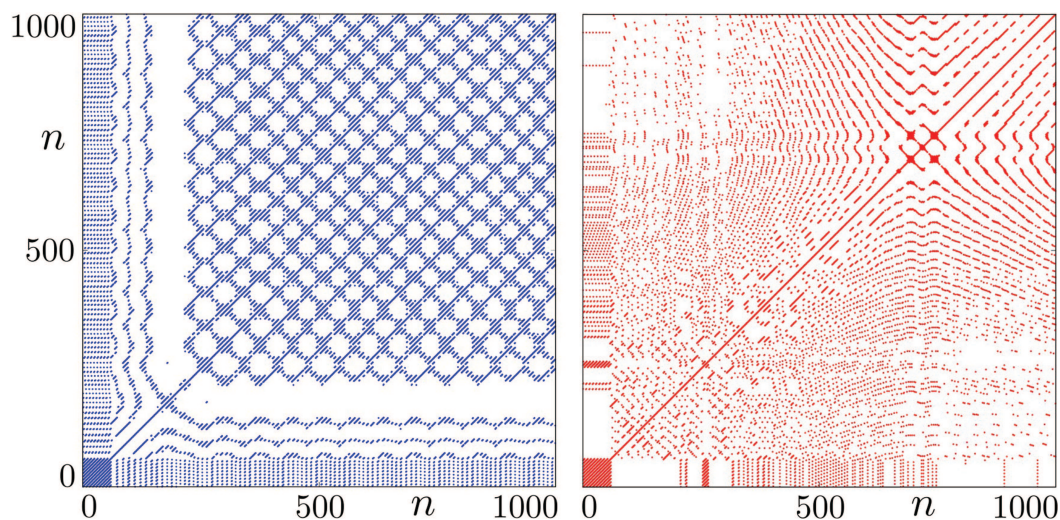
FIG. 19. RPs with $\varepsilon = 0.05$ for two particular trajectories of the UM. In blue, the trajectory started at $(x_0, y_0) = (x_0^h, y^*)$ (left), and in red, the trajectory started at $(x_0, y_0) = (x_0^l, y^*)$ (right).

by red and light-red colors above the blue manifold. In Fig. 15, we display the RP of this same particular orbit.

The RP of this particular orbit started in the close vicinity of the period 7 UPO, portrayed in Fig. 15, exhibits peculiar patterns. Initially, the RP shows a pure period behavior until around 60 iterations of the map, as amplified by the highlighted back square on the right. This periodic motion is when the orbit is still exactly at the position of the period 7 UPO, evidenced also by the distance between the initial diagonal lines $d_n = 7$. After sufficient long iteration time ($n \gtrsim 200$), the RP is dominated by patterns of complex dynamical behavior. Comparing with Fig. 14, at that time, the orbit explores the upper chaotic region composed of strong mixed structures, as its motion is confined to a thin chaotic layer between high periodicity KAM islands.

Now, following what was performed to the SM and SFUM, we place an ensemble E of 1000 ICs around the calculated UPO in the UM. For that, $y_0^E = y^*$ is fixed and we vary the position of x_0 only after the 12th valid digit of the calculated x^*. Thus, the ensemble is formed by a dense small line at $x_0^E \in [1.724\,770\,290\,892, 1.724\,770\,290\,894]$. We define again a relative distance, taking as a reference the x_0 of the orbit shown in Figs. 14 and 15, as $\Delta^{IC} = (x_0^E - x_0) \times 10^{13}$. In Fig. 16, we show the computed RR for all 1000 trajectories, iterated until $N = 1000$, in function of the defined relative distance in reference to x_0.

Analogously to other systems, the analysis made in Fig. 16 provides particular coordinates of the initial condition x_0 in which the orbit has high or low RR. Specifically, for $\varepsilon = 0.05$, we highlight in blue the value of $x_0 = x_0^h = 1.724\,770\,290\,893\,888$ and in red $x_0 = x_0^l = 1.724\,770\,290\,892\,971$, respectively, related to the highest and lowest values of RR. First, as done for the SFUM, it is possible to find an average RR for the ensemble, which

is $\langle RR \rangle = 1.784\,541$ for $\varepsilon = 0.05$ and consider the corrected $\tilde{RR} = RR - \langle RR \rangle$ in the next analysis. In Fig. 17, we amplify phase space of the UM for better visualization on the region of interest, showing via the colour axis the computed $\tilde{RR}$ for all trajectories in E.

Corroborating the approach for the SFUM, again the trajectories colored by their $\tilde{RR}$ differentiate regions of high and low recurrences on phase space of the UM. Note that the chaotic area is covered mostly by red orbits, indicating a low recurrence region, and regions surrounding the KAM islands are covered by blue orbits, indicating high recurrence in connection to stickiness. In addition to this analysis, we can verify the dynamical behavior of two particular orbits provided in Fig. 16. Figure 18 shows the evolution of the orbit with (x_0^h, y^*) on the left panel and the orbit with (x_0^l, y^*) on the right panel.

Similarly to the analysis for the SFUM, the orbit started at (x_0^h, y_0), in one hand, rapidly goes toward a region with many small KAM islands where it gets trapped in their surroundings until the end of its evolution. In another hand, the orbit started at (x_0^l, y_0) explores noticeably more the chaotic area, visiting different regions of phase space. In terms of transport and diffusion in phase space,[37] this result suggests that these particular chaotic trajectories, although started extremely close to each other, have completely distinct dynamical evolution until the maximum iteration time. In that regard, these two dynamics can be further analyzed considering the different transport properties and diffusion characteristics such as MSD and diffusion exponents. These further analyses will be addressed in another opportunity.

Furthermore, considering that $N = 1000$ was set as their maximum iteration time, it is possible to show the RPs of these particular trajectories.[38] Figure 19 displays those RPs following the
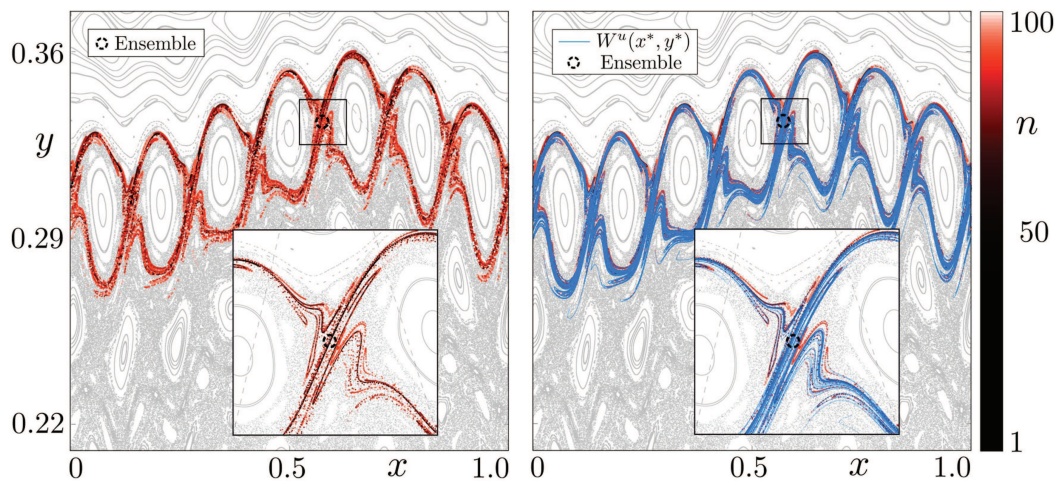
FIG. 20. Evolution of an ensemble of 1000 ICs in the phase space of the UM (left) and the computed invariant unstable manifold outlined in blue for comparison (right). The ensemble's initial position is highlighted by the dashed circle (out of scale). The color axis shows the iteration time for all trajectories.

defined palette throughout the text as blue for high and red for low recurrence cases.

Initially both RPs displayed in Fig. 19 reveal the same squared region related to the pure periodic motion, as discussed early for Fig. 15. After that, the two RPs differs widely from each other. The blue trajectory rapidly goes toward a region of strong quasi-periodic behavior, as its RP becomes dominated by patterns like the ones that can be observed at the end of the RP in Fig. 15. The red one, by its turn, shows patterns of rather complex dynamical behavior, exhibiting structures comparable to the ones shown by the green orbit in Fig. 3, that indeed corresponds to the same region of phase space. Comparing the RPs in Fig. 19 to their evolution in Fig. 18, it is possible to visualize the correlation between the displayed patterns and the correspondent regions in phase space on specific iteration intervals.

As a final visual comparison for the UM, we depict in Fig. 20 the evolution of all 1000 orbits in E considering only 100 iterations and the invariant unstable manifold W^u associated with the UPO at (x^*, y^*). As shown for the SM in Fig. 9, the evolution up to 100 iterations of a large ensemble of ICs placed in a neighborhood of a UPO shall follow the path outlined by the invariant unstable manifold of that UPO.

Indeed, as expected, the ensemble's evolution closely follows the outlined manifold as evidenced in Fig. 20. Particularly, the dark-red and red orbits, related to the interval between 50 and 100 iterations, still agree to the manifold path, implying that for even relative higher iterations the ensemble is still evolving accordingly to the manifold influence.

IV. GENERAL DISCUSSIONS AND CONCLUSIONS

As a general discussion regarding the numerical observations presented in the last section, we propose that the following method

can be used specifically to illustrate the presence of regions of stickiness in general non-linear Hamiltonian systems. Essentially, the method requires the following:

(1) A well-defined mixed phase space, as depicted in light-gray on the background of all phase space figures, in which it is possible to determine coordinates of the chaotic sea or at least a portion of chaotic region.
(2) Knowing the coordinates of ICs that provide chaotic trajectories, it is possible to define an ensemble E of M ICs around some particular region of phase space.
(3) Evolving all M trajectories until a given N maximum number of iterations of the dynamical equations, it is possible to compute their RR via Eq. (2), considering also a given value for the recurrence threshold distance ε.
(4) Once calculated the RR for each trajectory in E, one can plot it as a function of IC positions, identifying coordinates in which RR is high. Here, it is possible to analyze changes in the ICs' positions in both x and y axes. Figures 6, 10, and 16 are examples of this procedure.
(5) Finally, it is possible to plot all trajectories in E colored by their respective values of RR. Hence, trajectories with high recurrence are distinguished from the others and, combined with phase space on the background, regions around KAM islands will be highlighted, indicating the orbits that experience stickiness in the considered time-frame. Figures 7, 11, and 17 are examples of this procedure.

Moreover, the described procedure can be adjusted to the particularities of the investigated system. For the SFUM and the UM, a corrected RR was proposed, and regions of low recurrence could be easily identified, revealing also particular trajectories that, although started from near ICs, evolve in rather different dynamical behaviors.

It was shown that the simplest recurrence quantification, namely, the *RR*, is suitable to differentiate finite-time chaotic trajectories in mixed phase spaces. Particularly, for the standard map, the recurrence analysis illustrates the well-known sensitivity to the ICs of chaotic orbits, and considering an ensemble of ICs placed in a particular region of phase space, it was possible to verify the underlying influence of an invariant unstable manifold. For the Fermi-Ulam model, it was possible to determine particular chaotic orbits, from a broad sample of initial phases, that explore the phase space rather differently compared to the average ensemble behavior. Finally, for the ergodic magnetic limiter map, a dense ensemble was set on a small neighborhood around an UPO, where complex dynamical behavior emerges, as evidenced by the computed RPs of trajectories in this region. These RPs are examples of the rich finite-time chaotic behavior experienced by these orbits, beginning with a pure periodic motion, where the periodicity of the UPO can be additionally inferred, and escaping toward other mixed regions of phase space, displaying unique recurrence patterns.

The finite-time recurrence analysis outlined in this work opens interesting questions regarding the dependence on control parameters such as the recurrence distance threshold ε, maximum iteration time N, and the exact coordinates of the ICs. In particular, the scaling behavior while varying ε for the computed *RR* as a function of the ICs, and the transport/diffusion properties of particular trajectories with similar ICs, but with distinct dynamical evolution could be addressed in additional works. Furthermore, the initial pure periodic behavior displayed by some trajectories started near the UPOs could be further investigated in order to understand the transition between the unstable periodic state to the rest of the chaotic dynamics.

AUTHOR DECLARATIONS
Conflict of Interest

The authors have no conflicts to disclose.

Author Contributions

Matheus S. Palmero: Conceptualization (lead); Methodology (lead); Software (lead); Writing – original draft (lead). **Iberê L. Caldas:** Funding acquisition (equal); Methodology (supporting); Resources (equal); Supervision (equal); Validation (equal); Writing – review & editing (equal). **Igor M. Sokolov:** Conceptualization (supporting); Funding acquisition (equal); Investigation (supporting); Methodology (supporting); Resources (equal); Validation (equal); Writing – review & editing (equal).

DATA AVAILABILITY

The data that support the findings of this study are available from the corresponding author upon reasonable request.

REFERENCES

[1] R. M. May, "Simple mathematical models with very complicated dynamics," Nature **261**, 459–467 (1976).
[2] E. Ott, "Goodness of ergodic adiabatic invariants," Phys. Rev. Lett. **42**, 1628–1631 (1979).
[3] G. M. Zaslavsky, *Chaos in Dynamic Systems* (Harwood Academic Publishers, 1985).
[4] A. J. Lichtenberg and M. A. Lieberman, *Regular and Chaotic Dynamics* (Springer, Berlin, 1992).
[5] V. Gelfreich, V. Rom-Kedar, K. Shah, and D. Turaev, "Robust exponential acceleration in time-dependent billiards," Phys. Rev. Lett. **106**, 074101 (2011).
[6] J. D. Meiss, "Thirty years of turnstiles and transport," Chaos **25**, 097602 (2015).
[7] D. J. Muraki and W. L. Kath, "Hamiltonian dynamics of solitons in optical fibers," Physica D **48**, 53–64 (1991).
[8] P. J. Morrison, "Hamiltonian description of the ideal fluid," Rev. Mod. Phys. **70**, 467–521 (1998).
[9] S. A. Astakhov, A. D. Burbanks, S. Wiggins, and D. Farrelly, "Chaos-assisted capture of irregular moons," Nature **423**, 264–267 (2003).
[10] S. S. Abdullaev, *Magnetic Stochasticity in Magnetically Confined Fusion Plasmas* (Springer, 2014).
[11] G. M. Zaslavsky, "Chaos, fractional kinetics, and anomalous transport," Phys. Rep. **371**, 461–580 (2002).
[12] J. D. Meiss, "Symplectic maps, variational principles, and transport," Rev. Mod. Phys. **64**, 795–848 (1992).
[13] E. G. Altmann, A. E. Motter, and H. Kantz, "Stickiness in hamiltonian systems: From sharply divided to hierarchical phase space," Phys. Rev. E **73**, 026207 (2006).
[14] G. Contopoulos and M. Harsoula, "Stickiness effects in chaos," Celestial Mech. Dyn. Astron. **107**, 77–92 (2010).
[15] Y.-C. Lai and T. Tél, *Transient Chaos: Complex Dynamics on Finite Time Scales* (Springer Science & Business Media, 2011), Vol. 173.
[16] L. A. Bunimovich and L. V. Vela-Arevalo, "Many faces of stickiness in Hamiltonian systems," Chaos **22**, 026103 (2012).
[17] M. Harsoula, K. Karamanos, and G. Contopoulos, "Characteristic times in the standard map," Phys. Rev. E **99**, 032203 (2019).
[18] L. A. Bunimovich, "Relative volume of Kolmogorov–Arnold–Moser tori and uniform distribution, stickiness and nonstickiness in Hamiltonian systems," Nonlinearity **21**, T13 (2008).
[19] J. P. Zbilut and C. L. Webber, "Embeddings and delays as derived from quantification of recurrence plots," Phys. Lett. A **171**, 199–203 (1992).
[20] N. Marwan, N. Wessel, U. Meyerfeldt, A. Schirdewan, and J. Kurths, "Recurrence-plot-based measures of complexity and their application to heart-rate-variability data," Phys. Rev. E **66**, 026702 (2002).
[21] Y. Zou, M. Thiel, M. C. Romano, and J. Kurths, "Characterization of stickiness by means of recurrence," Chaos **17**, 043101 (2007).
[22] Y. Zou, R. V. Donner, M. Thiel, and J. Kurths, "Disentangling regular and chaotic motion in the standard map using complex network analysis of recurrences in phase space," Chaos **26**, 023120 (2016).
[23] V. Lucarini, D. Faranda, A. Freitas, J. Freitas, M. Holland, T. Kuna, M. Nicol, M. Todd, and S. Vaienti, *Extremes and Recurrence in Dynamical Systems* (Wiley, 2016).
[24] B. V. Chirikov, "A universal instability of many-dimensional oscillator systems," Phys. Rep. **52**, 263–379 (1979).
[25] E. Fermi, "On the origin of the cosmic radiation," Phys. Rev. **75**, 1169–1174 (1949).

[26] E. D. Leonel, P. V. E. McClintock, and J. K. L. da Silva, "Fermi-Ulam accelerator model under scaling analysis," Phys. Rev. Lett. **93**, 014101 (2004).

[27] T. Pereira and D. Turaev, "Exponential energy growth in adiabatically changing Hamiltonian systems," Phys. Rev. E **91**, 010901 (2015).

[28] K. Ullmann and I. L. Caldas, "A symplectic mapping for the ergodic magnetic limiter and its dynamical analysis," Chaos Solitons Fractals **11**, 2129–2140 (2000).

[29] C. W. Horton and S. Benkadda, *ITER Physics* (World Scientific, 2015).

[30] I. L. Caldas, J. M. Pereira, K. Ullmann, and R. L. Viana, "Magnetic field line mappings for a tokamak with ergodic limiters," Chaos Solitons Fractals **7**, 991–1010 (1996).

[31] E. C. da Silva, I. L. Caldas, and R. L. Viana, "Ergodic magnetic limiter for the TCABR," Braz. J. Phys. **32**, 39–45 (2002).

[32] Here, a technical note is relevant: As the difference $(q_0^E - q_0^*)$ is extremely small, we are approaching the maximum precision of a double in computer simulations, so the ensemble's size needs to be fitted considering this restriction.

[33] A. M. Ozório de Almeida, N. de Leon, M. A. Mehta, and C. C. Marston, "Geometry and dynamics of stable and unstable cylinders in Hamiltonian systems," Physica D **46**, 265–285 (1990).

[34] V. M. de Oliveira, P. A. Sousa-Silva, and I. L. Caldas, "Order-chaos-order and invariant manifolds in the bounded planar Earth–Moon system," Celestial Mech. Dyn. Astron. **132**, 1–17 (2020).

[35] D. Ciro, I. L. Caldas, R. L. Viana, and T. E. Evans, "Efficient manifolds tracing for planar maps," Chaos **28**, 093106 (2018).

[36] A. L. P. Livorati, C. P. Dettmann, I. L. Caldas, and E. D. Leonel, "On the statistical and transport properties of a non-dissipative Fermi-Ulam model," Chaos **25**, 103107 (2015).

[37] M. S. Palmero, G. I. Díaz, P. V. E. McClintock, and E. D. Leonel, "Diffusion phenomena in a mixed phase space," Chaos **30**, 013108 (2020).

[38] Since it was chosen $N = 10^4$ for the SFUM, the RPs of the trajectories were rather large, making their visual representation not so clear, so we decided to overlook them.